AJNR

# MR imaging of the craniocervical junction.

B C Lee, M D Deck, J B Kneeland and P T Cahill

*AJNR Am J Neuroradiol* 1985, 6 (2) 209-213
http://www.ajnr.org/content/6/2/209

# MR Imaging of the Craniocervical Junction

Benjamin C. P. Lee[1]
Michael D. F. Deck
J. Bruce Kneeland
Patrick T. Cahill

**Craniocervical junctions in 35 abnormal and 10 normal subjects were studied with a 0.5 T superconducting magnetic resonance imaging system. Sagittal spin echo with 30 msec echo times and 500 msec repetition times constituted the most informative imaging plane and sequence. The anterior aspect of the foramen magnum was well delineated; the posterior margin was less constant in appearance. Compression and distortion of the medulla and upper cervical cord by bony and extramedullary lesions were seen easily. Intramedullary cysts were differentiated from solid tumors, but ventricular communication was evaluated less successfully because of partial-volume effect of the sections. Cerebellar ectopias were detected in some asymptomatic patients.**

Neurologic symptoms from disorders of the craniocervical junction are caused by compression and distortion of neurologic structures. Although plain films and computed tomographic (CT) scans are precise in defining bony abnormalities, the medulla and cervical spinal cord are virtually never shown well on CT scans. Intrathecal contrast myelography or CT is usually required for delineation of the medulla and cervical spinal cord [1, 2]. These procedures are performed only when neurologic deficits are pronounced [3, 4]. Magnetic resonance (MR) imaging promises to be an excellent noninvasive method of evaluating abnormalities of this region [5–13].

## Subjects and Methods

We studied 35 patients with craniocervical abnormalities (table 1). All were symptomatic, exept for six with Chiari I malformations. Ten normal sagittal MR scans were reviewed from patients without craniocervical symptoms.

MR scanning was performed using a Technicare 0.5 T scanner. CT was performed using either a GE 8800, 9800, or another third- or fourth-generation scanner. Preliminary sagittal views with several different spatial offsets were performed using a spin-echo (SE) technique with a short echo delay time (TE) of 30 msec and a repetition time (TR) of 200 msec (SE 200/30). The scans were reviewed, and the location corresponding to the midline was selected for more detailed evaluation using SE 500/30 in all cases. Multiple axial SE 1500/90 sections were obtained in all cases, except in two patients with brainstem atrophy and rheumatoid arthritis, who were too ill to tolerate more than the sagittal imaging. Additional single sagittal SE 1500/90 sections were obtained in all cases of arachnoid cyst, vertebral ectasia, tumor, and syrinx. Single inversion-recovery (IR) sections using inversion times (TIs) of 450 msec and TRs of 1500 msec, IR 1500/450, were obtained in a few selected cases where better definition of the cerebellar tonsils was required. Single sections were 10 mm thick and multiple sections were 8 mm thick. Eight simultaneous, noncontiguous sections with slice intervals of 8 mm were obtained, each with multisection single-echo technique; the sections were repeated with spatial offset to achieve contiguous visualization.

Received June 20, 1984; accepted after revision September 19, 1984.

[1] All authors: Department of Radiology, New York Hospital–Cornell Medical Center, 525 E. 68th St., New York, NY 10021. Address reprint requests to B. C. P. Lee.

*AJNR* 6:209–213, March/April 1985
0195–6108/85/0602–0209

TABLE 1: **Types of Craniocervical Abnormalities in Patients Evaluated with Magnetic Resonance Imaging**

| Pathology | No. of Cases |
|---|---|
| None | 10 |
| Upward herniation of dens | 2 |
| Fracture of dens | 1 |
| Rheumatoid arthritis | 3 |
| Meningioma | 2 |
| Arachnoid cyst | 3 |
| Giant aneurysm | 1 |
| Vertebral ectasia | 1 |
| Chiari I | 10 |
| Syringomyelia | 4 |
| Intramedullary tumor | 4 |
| Brainstem atrophy | 4 |
| Total | 45 |

## Results and Discussion

### *Technique*

Sagittal views provide direct visualization of the brainstem, cerebellar tonsils, and upper cervical spine. The resolution is vastly superior to reformatted plain CT views and comparable to metrizamide sagittal reformatted views. However, axial views are required whenever asymmetric distortion or displacement of these structures is suspected. MR views in this plane are free of artifacts and comparable to direct metrizamide CT studies. The choice of imaging sequences is dictated by the need to image structures with maximal anatomic detail and detection of altered signal of lesions. In our evaluations SE technique using short TEs and TRs (SE 500/30) provided the best anatomic detail. With this sequence, which has some T1 data, the cerebrospinal fluid (CSF) in the subarachnoid space and the fourth ventricle is of decreased signal intensity, so that the interfaces between it and the brainstem and cerebellum are clearly defined. Shorter TR sequences, such as in SE 200/30, contain more T1 information, but unfortunately have increased noise and are suboptimal for anatomic evaluations. Conversely, with longer TRs, such as SE 2000/30, CSF signal approaches that of neural tissues due to the T2 contribution of CSF. This often results in poor separation of these structures, even though there is improvement in the signal-to-noise (S/N) ratio.

SE techniques with longer TEs are sensitive for detecting abnormalities that alter T2 relaxation. The loss of signal may be compensated partly by increasing the TR. In the lumbosacral region, it is possible to render the subarachnoid space of increased signal by using very long TEs and TRs. Our studies of the craniocervical region using similar techniques are unsatisfactory because of poor S/N ratios and impractically long scanning times. The optimal compromise sequence with our system appears to be SE 1500/90, which detects changes of signal in most posterior fossa lesions despite lack of differentiation of brain and CSF. IR is seldom useful as the primary technique for evaluating craniocervical lesions, but is sometimes useful in revealing changes of T1 that are not detected with the routine SE 500/30 sequence.

### *Normal Appearances*

The foramen magnum is clearly seen on plain radiographs and geometric tomography. Since cortical bone has no signal on MR images and appears similar to subarachnoid space on short SE techniques (SE 500/30), the posterior margin of the foramen magnum is seldom identified. The transverse ligament behind the dens and the anterior longitudinal ligament, however, are usually visible (fig. 1). Although it is possible to increase the signal of CSF compared with cortical bone by increasing the TE and TR in SE techniques, the resulting loss of resolution usually makes it impossible to image the edge of the foramen [14, 15]. The size of the marrow cavity within vertebrae is variable, and this results in an unpredictable configuration of the tip of the dens and anterior arch of the axis. The posterior margin of the dens, however, appears to be consistently well defined, so that subtle changes may be evaluated. A variable amount of fat is constantly present between the tip of the clivus and the anterior margin of the dens (fig. 1).

The fourth ventricle, cerebellar tonsils, medulla, and cervical spinal cord are defined excellently on both sagittal and axial SE 500/30 images. Subtle distortions are thus easily appreciated.

### *Bone Lesions*

Basilar invagination, fracture, rheumatoid erosion, and upward displacement of the dens into the posterior fossa may produce neurologic symptoms by mechanical compression of the medulla and upper cervical spinal cord; this is demonstrable with myelography and metrizamide CT. These invasive procedures may be dangerous in the presence of neck instability and should be avoided unless surgical treatment is contemplated. Fracture of the dens is sometimes visible on sagittal MR using SE 500/30 scans (fig. 2). Congenital upward herniation of the dens into the foramen magnum causing medullary compression is easily demonstrated (fig. 3). Small erosions of the posterior part of the dens are seen equally well on MR and CT images (fig. 4), but changes of the odontoid tip are difficult to evaluate due to the variable normal appearances of this structure.

### *Extradural Lesions*

Tumors of the foramen magnum are difficult to recognize on conventional CT scans, unless there are bony changes, calcification, or alterations of attenuation with contrast enhancement. Supine myelography and reformatted sagittal metrizamide CT scans are usually required for diagnosis and evaluation of the spinal cord and medullary compression [16, 17]. These lesions are imaged on sagittal MR even when contrast of the tumor differs little from surrounding structures (fig. 5). The signal of the foramen magnum meningioma did not alter with different SE and IR techniques. This lack of change of signal intensity is consistent with our experience with meningiomas in other parts of the central nervous system [18]. MR imaging is especially useful in postoperative cases,

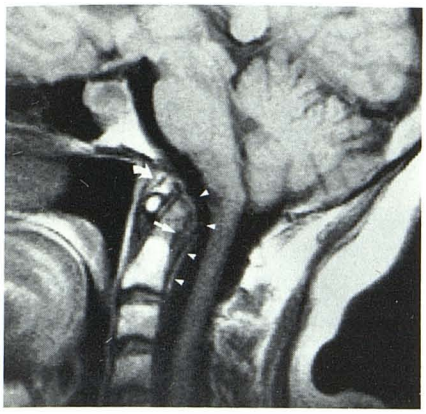

Fig. 1.—Sagittal SE 500/30 image in normal patient. Absence of signal of cortical bone, indistinguishable from subarachnoid space, makes it difficult to define posterior margin of foramen magnum. Dens has irregular appearance. Longitudinal (*arrowheads*) and transverse (*straight arrow*) ligaments. Fat, with increased signal, between tip of clivus and dens (*curved arrow*).

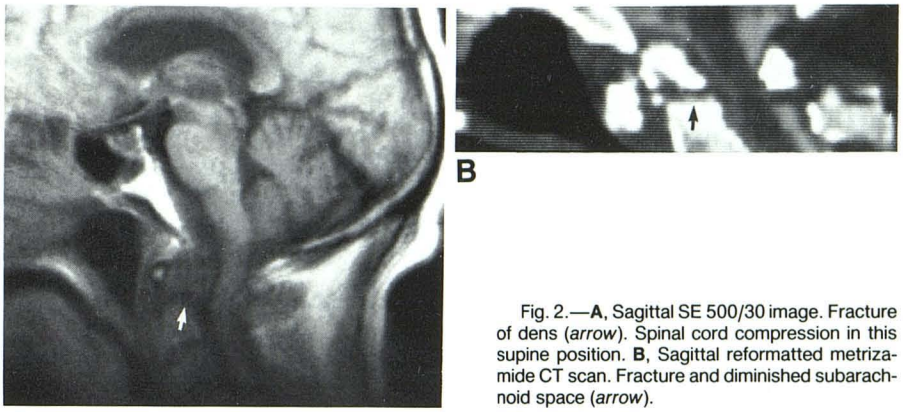

Fig. 2.—**A**, Sagittal SE 500/30 image. Fracture of dens (*arrow*). Spinal cord compression in this supine position. **B**, Sagittal reformatted metrizamide CT scan. Fracture and diminished subarachnoid space (*arrow*).

Fig. 3.—Congenital abnormality (clinical diagnosis). **A**, Sagittal SE 500/30 image. Upward herniation of dens into foramen magnum. Compression of medulla.

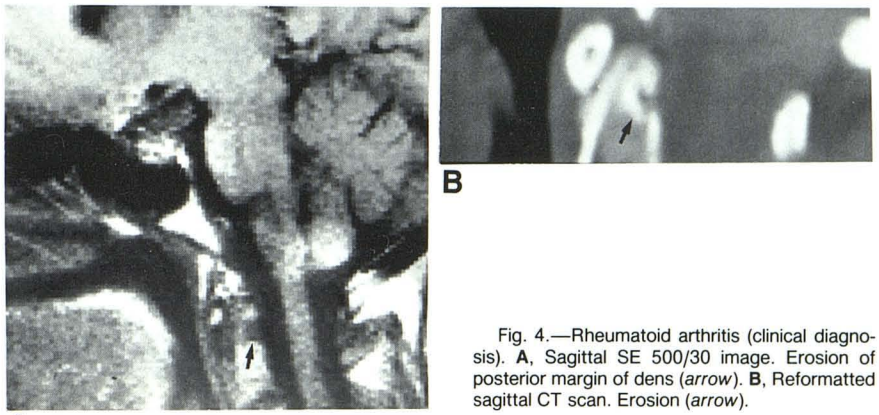

Fig. 4.—Rheumatoid arthritis (clinical diagnosis). **A**, Sagittal SE 500/30 image. Erosion of posterior margin of dens (*arrow*). **B**, Reformatted sagittal CT scan. Erosion (*arrow*).

where metallic surgical material often produces unacceptable artifacts on CT scans; MR artifacts are usually much less extensive.

*Extramedullary Lesions*

Posterior fossa cysts may be neoplastic or arachnoid in origin and are often indistinguishable on CT scans [19]. Our data indicate that arachnoid cysts invariably have a pointed inferior margin that may extend into the posterior cervical canal and may displace the cerebellar tonsils below the foramen magnum (fig. 6). There are varying degrees of compression of the cerebellar hemispheres and the spinal cord.

Giant aneurysms and ectasia of the vertebral arteries may cause brainstem and cervical cord compression; they have characteristic configurations. Although hematoma within the vessels results in a bright signal in all imaging sequences, slight increase of signal has to be interpreted with caution, as it may be due to sluggish flow and not to a clot [20, 21].

*Intramedullary Lesions*

Chiari I malformations may give rise to protean clinical symptoms, which are seldom sufficient to warrant invasive intrathecal contrast studies [22, 23]. Such deformities are easily visible on sagittal MR images [24] and are often detected during routine examinations of patients with unrelated symptoms (fig. 7). The precise extent of the cerebellar ectopia may be difficult to determine due to difficulty in defining the

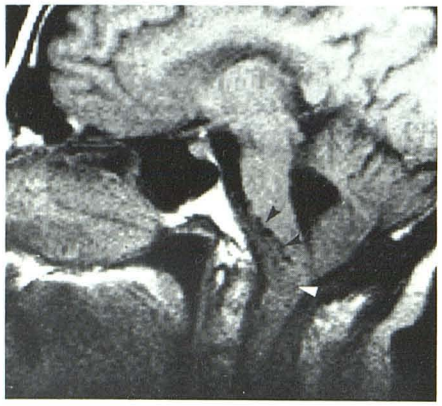

Fig. 5.—Meningioma (surgical pathology). Sagittal SE 500/30 image. Extrinsic mass in anterior part of posterior fossa and foramen magnum compresses medulla and cervical spinal cord (*arrowheads*). Tumor and medulla have similar signal intensity.

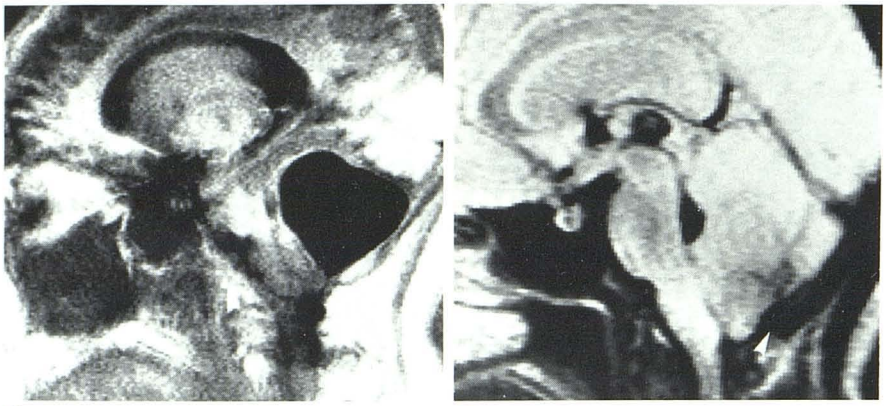

A B

Fig. 6.—Arachnoid cyst (surgical pathology). **A**, Sagittal IR 1500/450 image. Cyst compresses cerebellum. Pointed inferior margin. **B**, SE 1500/90 image. Herniation of cerebellar tonsil (margin of foramen magnum) (*arrowhead*).

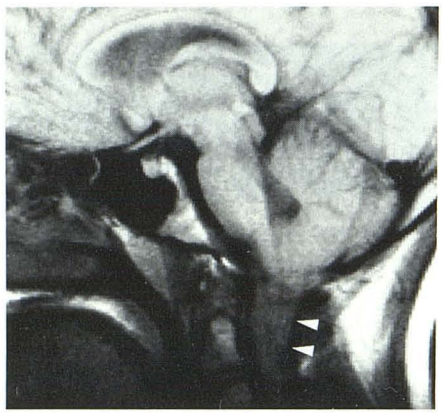

Fig. 7.—Chiari I malformation (clinical diagnosis). Sagittal SE 500/30 image. Extension of cerebellar tonsils into cervical subarachnoid space (*arrowheads*) inseparable from cervical cord.

A B

Fig. 8.—Syringomyelia (clinical diagnosis). **A**, Axial SE 500/30 image. Large cavity within upper cervical cord. **B**, Sagittal image. Extension of central cavity into medulla, which is enlarged (*arrowheads*).

exact margin of the foramen magnum. The degree of subarachnoid space narrowing caused by the ectopia is likewise difficult to assess, unless there is pronounced brainstem and cord compression. The clinical significance of small degrees of tonsillar ectopia is uncertain unless associated with hydromyelia [25, 26].

Spinal cord enlargement is caused by intramedullary tumors or cavities within the cord. A firm diagnosis of hydromyelia and syringomyelia is made only when the cavities are visible on plain CT or fill with intrathecal contrast material [27–30]. It is uncertain what proportion of such cavities is missed by conventional radiologic studies [29]. Our limited experience suggests that MR is excellent in demonstrating such cavities (fig. 8). The best technique is SE 500/30. Very long TEs (120 msec or more) may produce more signal from the subarachnoid space and fluid cavities than from the spinal cord, but result in unacceptable loss of spatial resolution. It is possible to image the upper limit of the cavity, and communication with the fourth ventricle may be shown (fig. 8). Small passages of communication with the ventricles cannot, however, be excluded if discrete channels are not observed due to the limited spatial resolution in the *Z* axis and partial-volume effect of the MR sections used. Small intramedullary cavities may not be visible for the same reason. Despite these limitations this study confirms that MR imaging is the method of choice for screening for suspected syringomyelia and hydromyelia.

Intramedullary tumors of the craniocervical junction may be extensions from primary cervical cord or medullary lesions. The signal intensity in our one case is mixed, but the significance of these appearances is uncertain (fig. 9). Tumor enlargement is easily distinguished from cord and brainstem atrophy, which may produce identical symptoms (fig. 10).

Fig. 9.—Glioma (clinical diagnosis). Sagittal SE 500/30 image. Enlargement of medulla and upper cervical spinal cord (*arrowheads*). Speckles of increased signal within tumor.

Fig. 10.—Olivopontocerebellar degeneration (clinical diagnosis). Sagittal SE 500/30 image. Small size of brainstem, spinal cord, and cerebellar vermis.

9 10


REFERENCES

1. Shapiro R. *Myelography*, 3d ed. Chicago: Year Book Medical, **1976**
2. Skalpe IO, Sortland O. Cervical myelography with metrizamide (Amipaque). A comparison between conventional and computer-assisted myelography with special reference to the upper cervical and foramen magnum region. *Neuroradiology* **1978**;16:275–278
3. Leo TS, Bergeron RT, Kricheff II, Benjamin MV. Metrizamide myelography for cervical spinal cord injuries. *Radiology* **1978**;129:707–711
4. Carol M, Ducker TB, Byrnes DP. Mini myelogram in cervical spinal cord tumor. *Neurosurgery* **1980**;7:219–224
5. Young IR, Bailes DR, Burl M, et al. Initial clinical evaluation of the whole body nuclear magnetic resonance (NMR) tomograph. *J Comput Assist Tomogr* **1982**;6:118–129
6. McGinnis BD, Brady TJ, New PFJ, et al. Nuclear magnetic resonance (NMR) imaging of tumors in the posterior fossa. *J Comput Assist Tomogr* **1983**;7:575–584
7. Bydder GM, Steiner RE, Thomas DJ, Marshall J, Gilderdale DJ, Young IR. Nuclear magnetic resonance imaging of the posterior fossa: 50 cases. *Clin Radiol* **1983**;20:173–188
8. Randell CP, Collins AG, Young IR, et al. Nuclear magnetic resonance imaging of posterior fossa tumors. *AJNR* **1983**;4:1027–1034, *AJR* **1983**;141:489–496
9. Lee BCP, Kneeland BJ, Deck MDF, Cahill PT. Posterior fossa lesions: magnetic resonance imaging. *Radiology* **1984**;153:137–143
10. Modic MT, Weinstein MA, Pavlicek W, Boumphrey F, Starnes D, Duchesneau PM. Magnetic resonance imaging of the cervical spine: technical and clinical observations. *AJNR* **1984**;5:15–22, *AJR* **1983**;141:1129–1136
11. Han JS, Kaufmann B, El Yousef SJ, et al. NMR imaging of the spine. *AJNR* **1983**;4:1151–1159, *AJR* **1983**;141:1137–1145
12. Norman D, Mills CM, Brant-Zawadzki M, Yeates A, Crooks LE, Kaufman L. Magnetic resonance imaging of the spinal cord and canal: potentials and limitations. *AJNR* **1984**;5:9–14, *AJR* **1983**;141:1147–1152
13. Modic MT, Weinstein MA, Pavlicek W. Nuclear magnetic resonance imaging of the spine. *Radiology* **1983**;148:757–762
14. Crooks LE, Mills CM, Davis PL, et al. Visualization of cerebral and vascular abnormalities by NMR imaging. The effects of imaging parameters on contrast. *Radiology* **1982**;144:843–852
15. Wehrli FW, MacFall J, Newton TH. Parameters determining the appearance of NMR images. In: Newton TH, Potts DG, eds. *Modern neuroradiology*, vol 2. *Advanced imaging techniques.* San Anselmo, CA: Clavadel, **1983**:81–118
16. Wickbom I, Hanafee W. Soft tissue anatomy within the spinal canal as seen on computed tomography. *Radiology* **1980**;134:649–655
17. Glanz S, Geehr RB, Duncan CC, Piepmeier JM. Metrizamide enhanced CT for evaluation of brainstem tumors. *AJNR* **1980**;1:31–34, *AJR* **1980**;134:821–824
18. Zimmerman RD, Fleming CA, Saint-Louis LA, Lee BCP, Manning JJ, Deck MDF. Magnetic resonance imaging of meningiomas. *AJNR* **1985**;6:149–157
19. Lee BCP. Intracranial cysts. *Radiology* **1979**;130:667–674
20. Kaufman L, Crooks L, Sheldon P, Hricak H, Herfkins R, Banks W. *Circulation* **1983**;67:251–257
21. Mills CM, Brant-Zawadzki M, Crooks LE, et al. Nuclear magnetic resonance: principles of blood flow imaging. *AJNR* **1983**;4:1161–1166, *AJR* **1984**;142:165–170
22. Saez RJ, Onofrio BM, Yanagihari T. Experience with Arnold-Chiari malformation, 1960–1970. *J Neurosurg* **1976**;45:416–422
23. Appleby A, Foster JB, Hankinson J, Hudgson P. The diagnosis and management of the Chiari anomalies in adult life. *Brain* **1968**;92:131–139
24. DeLaPaz RL, Brady TJ, Buonanno FS, et al. Nuclear magnetic resonance (NMR) imaging of Arnold-Chiari type I malformation with hydromyelia. *J Comput Assist Tomogr* **1983**;7:126–129
25. Banerji NK, Miller JHD. Chiari malformation presenting in adult life: its relationship to syringomyelia. *Brain* **1974**;97:157–168
26. du Boulay G, Shah SH, Currie JL, Logue VL. The mechanism of hydromyelia of Chiari type I malformation. *Br J Radiol* **1974**;49:579–587
27. DiChiro G, Axelbaum SP, Schellinger D, et al. Computerized axial tomography in syringomyelia. *N Engl J Med* **1975**;292:13–16
28. Forbes W StC, Isherwood I. Computer tomography in syringomyelia and the associated Arnold-Chiari type I malformation. *Neuroradiology* **1978**;15:73–78
29. Bonafe A, Ethier R, Melancon D, Belanger G, Peters T. High resolution computer tomography in cervical syringomyelia. *J Comput Assist Tomogr* **1980**;4:42–47
30. Aubin ML, Vignaud J, Jardin C, Bar D. Computed tomography in 75 clinical cases of syringomyelia. *AJNR* **1981**;2:199–204